# Electron-Rich Bonding and the Importance of s,p Mixing as One Moves Across a Period: A Lesson from the LiSn System

**Andrea Ienco, Roald Hoffmann,* and Garegin Papoian**

*Contribution from the Department of Chemistry and Chemical Biology, Cornell University, Ithaca, New York, 14853-1301*

*Received September 5, 2000. Revised Manuscript Received December 4, 2000*

**Abstract:** The electronic structure of an unusual LiSn phase (computed using band structure calculations in the framework of the extended Hückel tight binding theory) is the starting point for a general analysis of the variation of electron-rich multicenter bonding across a period. The LiSn crystal structure of Müller and Schäfer in question contains 2D slabs of Sn atoms arranged as microscopic stairs and intercalated by Li atoms. Discrepancies between an electron count derived from a recent extension of the Zintl−Klemm rules to electron-rich systems ($5^2/_3$ electrons) and the experimental one (5 electrons for the Sn sublattice) and other failures of chemical "common sense" emerge in the analysis. The key for interpretation of a series of puzzling results was found in the comparative analysis of the Sn net with other main group element hypervalent slabs. Increasing s,p-mixing as one moves from the right to the left side of the same row of the periodic table is responsible for these effects. The result is that a lower electron count is found in the Sn slabs relative to the one expected from the extended Zintl−Klemm theory. The effect should also occur in discrete molecules. We also showed that the Li atoms have a role in the determination of the final structure, not only because of their small size but also through the degree of the electron transfer to the Sn sublattice.

## Introduction

The lithium−tin system is a model for the electrochemically active interface of lithium ion batteries, now one of the most important rechargeable power sources for portable electronic devices.[1] Lithium and tin are known to form several binary compounds,[2] some of which have unusual, unexpected structures. Consider the (1:1) LiSn phase. Assuming $Li^+$, the tin atoms carry a formal negative charge and are then isoelectronic with group V elements. Following the Zintl−Klemm concept,[3] a three-connected cluster or three-connected network, common for group V elements, is the type of structure expected.

But *neither* of the two reported LiSn structures[4] is a three-connected one. The following shows a drawing of the two structures (the lithium atoms are omitted for the sake of clarity).

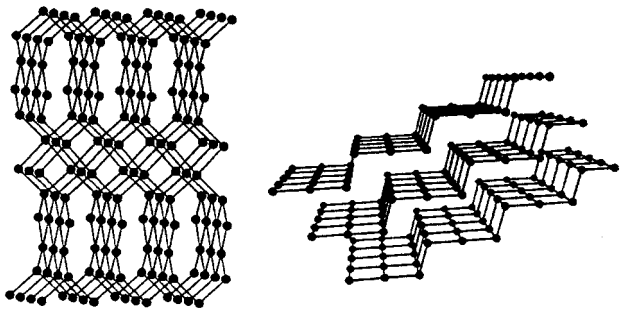

**1**

The left one[4a] is isotypic to high-pressure LiGe;[5] it contains eight-membered rings with two different types of Sn atoms. One atom has a pseudotetrahedral environment and the other has a distorted square-planar environment with two short and two long distances. The bonding in this structure was analyzed by one of us in a previous paper.[6]

The other LiSn structure[4b] consists of a series of infinite 2D tin layers intercalated by the lithium atoms. The distance between two layers of tin atoms is 4.17 Å. The long interslab separation suggests that there is little covalent bonding between the two layers. As seen in **1**, each tin slab is like a microscopic stair with a tread of 6.32 Å and a riser of 3 Å. Structure **2** labels

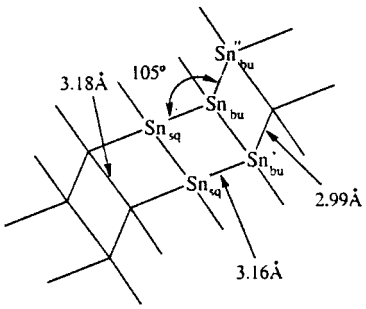


**2**

the atoms and shows the interatomic distance in a layer. Two lines of Sn atoms are spaced 3.18 Å apart.

* To whom the correspondence should be addressed. e-mail: rh34@cornell.edu.

(1) Courtney, I. A.; Tse J. S., Mao O., Hafner J., Dahn J. R. *Phys. Rev. B* **1998**, *58*, 15583.

(2) The reported LiSn compounds are the following. (a) $Li_2Sn_5$: Hansen D. A. *Acta Crystallogr. Sect. B* **1978**, *25*, 2392. (b) $Li_7Sn_3$: Müller, W. *Z. Naturforsch.* **1974**, *30B*, 1. (c) $Li_5Sn_2$: Müller, W.; Schäfer, H. *Z. Naturforsch.* **1973**, *28B*, 246. (d) $Li_{13}Sn_5$: Frank, U.; Müller, W.; Schäfer, H. *Z. Naturforsch.* **1975**, *30B*, 1. (e) $Li_7Sn_2$: Frank, U.; Müller, W.; Schäfer, H. *Z. Naturforsch.* **1975**, *30B*, 6

(3) Zintl, E. *Angew. Chem.* **1939**, *53*, 1.

(4) (a) Blase, W.; Cordier G. *Z. Kristallogr.* **1990**, *193*, 317. (b) Müller, W.; Schäfer, H. *Z. Naturforsch.* **1973**, *28B*, 246.

(5) Volk, R.; Müller, W.*Z. Naturforsch.* **1978**, *30B*, 593.

(6) Sherwood, P.; Hoffmann R. *J. Am. Chem. Soc.* **1990**, *112*, 2881.

10.1021/ja0032576 CCC: $20.00 
Published on Web 02/14/2001

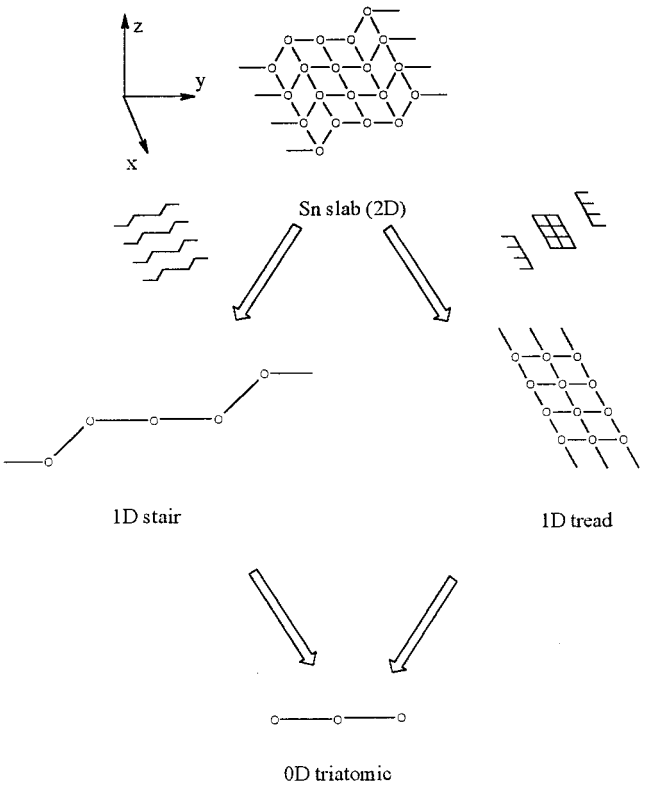


**Figure 1.** "Retrotheoretically" decomposing the 2D slab. Two possible ways of moving back to the 0D triatomic molecule are shown. On the left side we cut the 2D stair slab in the direction of "climbing of the stair", on the right side we break the stair into treads. Both of the 1D stair and 1D tread are after that decomposed into 0D triatomic molecules.

There are two kinds of Sn atoms in each slab. One ($Sn_{sq}$) is in a quasi-square-planar environment; the other ($Sn_{bu}$) in a "butterfly" or bent environment (one Sn−Sn−Sn angle is 105°). The distance between the planar and the butterfly Sn atoms is 3.16 Å and that between two butterfly Sn atoms is 2.99 Å. For calibration, a normal Sn−Sn single bond distance is around 2.8 Å; distances around 3.1 Å are quite common in binary and ternary Sn phases and are indicative of Sn−Sn electron-rich bonds.[7] In this paper, we examine the electronic structure of this second LiSn phase in order to understand better the bonding in it. What emerges is not just a picture of the bonding, but an important insight into the role of s,p mixing in determing structure as one moves across a period.

**The Expected "Magic" Electron Count of the 2D Slab in LiSn.** In a previous paper,[7] two of us developed an extension of the classical Zintl−Klemm electron counting rules[3] for electron-rich, hypervalent phases. In the remainder of the paper, we will call this electron counting algorithm the "extended Zintl-Klemm" count. Let us see where this type picture of the LiSn crystal takes us. The approach we choose is to start from the 3D crystal and "retrotheoretically" decompose it to move step by step to a molecular compound, a 0D object. Then the full structure is reassembled, reversing the process. While this *Aufbau* may seem tedious, it is, we think, an informative way of connecting different pieces of the chemical universe. The picture in Figure 1 describes the later steps of that process.

First, we eliminate the lithium cations, leaving a 3D lattice of $Sn^{1-}$ slabs. We take this Sn sublattice apart into 2D slabs (assuming little interaction between slabs; this will be tested). There are several ways to subdivide the 2D slab. In Figure 1, we show two of them. In the first case, we cut the slab in the direction of "climbing of the stair;" in the second case, we break the stair into treads. These two approaches, each leading to 1D structures, will eventually provide us different and complementary information on the electronic structure of the 2D sheets.

Let's call these 1D structures a "1D stair" and a "1D tread". How can we decompose them further? Each structure can be built from a triatomic main group unit by "end-on" or "sideways" stacking, indicated toward the bottom of Figure 1.

Let us now reverse this procedure, in an *Aufbau* of the complete slab. The aim is to see what is the optimum electron count expected. We begin with the linear triatomic. A model is $I_3^-$, $XeF_2$, or $Te_3^{4-}$; the Sn analogue would be $Sn_3^{10-}$. The qualitative electronic structure of such a system is shown in **3**.

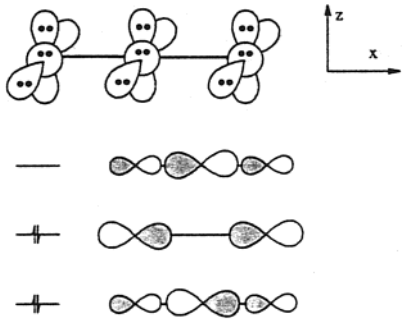


**3**

Assuming little s,p mixing for the moment[7] (we will have to return to this), each atom has 6 electrons in s and $p_y$, $p_z$ orbitals. The remaining three $p_x$ orbitals form a classical hypervalent three-center electron-rich orbital system, occupied by 4 electrons. The net electron count is 18 + 4 = 22 electrons per 3 atoms.

Imagine sideways coupling of such units to form a 1D tread structure **4**. When $p_y$ lone pairs are fully occupied (22 electrons

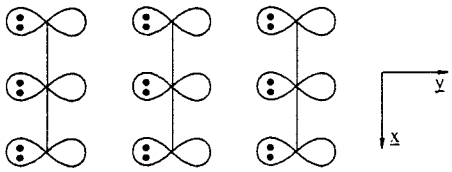


**4**

per 3 atoms), one should only get repulsion, indicated schematically by the lone pairs impacting each other in **4**. To achieve optimum (electron-rich) bonding along *y*, one needs to oxidize each $p_y$ lone pair by 1 electron.[8] This gets us to 19 electrons per 3 atoms.

The assembly of the 2D slab involves covalent bond formation roughly along *z*, as shown in **5**. Again keeping the

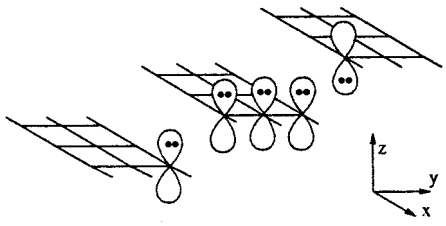


**5**

electron count at 19 would lead to repulsion of corresponding lone pairs. Oxidation by 1 electron at each "terminal" atom of a triatomic building block would give good bonding. The

(7) Papoian, G.; Hoffmann, R. *Angew. Chem., Int. Ed.* **2000**, *39*, 2408.

(8) Papoian, G.; Hoffmann R. *J. Solid State Chem.* **1998**, *139*, 8.

resultant electron count is $(19 - 2) = 17$, or $5^2/_3$ electrons per main group atom in order to form new bonds.

Now let us assemble the slab in the other way. The formation of a 1D stair from a 0D triatomic is shown in **6**. The optimum

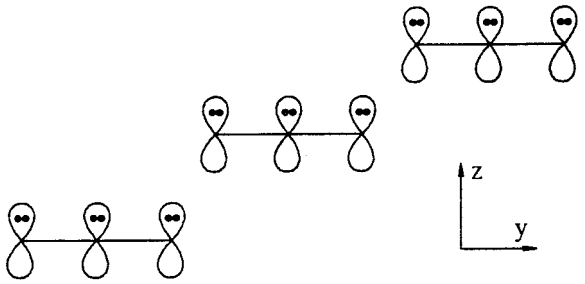


**6**

electron count for the 1D stair is for $22 - 2 = 20$ electrons, oxidizing the system by 1 electron at each terminal atom.

The 2D slab is reassembled by bringing these 1D stairs together along *y*, as shown in **7**. This again encounters repulsion

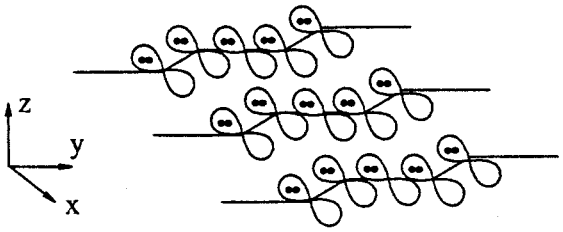


**7**

unless there is oxidation by 1 electron at *each* center (from $p_x$), leading to an electron count of $20 - 3 = 17$ per 3 atoms or again $5^2/_3$ per main group atom.

Either way, (it would have been a surprise if the outcome had been different) the extended or electron-rich Zintl−Klemm counting protocol leads to $5^2/_3$ electrons per tin, which is in excess of the actual 5 electrons the structure possesses in LiSn. We will return to this point below; it will give us important insight into a new aspect of electron-rich multicenter bonding in extended structures.

There is one more point to make relevant to the extended Zintl−Klemm count of $5^2/_3$ electrons per atom. This is that the *Aufbau* leads to a distinction in electron count at the center of the tread (the square planar atom) and at the ends of the tread (the butterfly atom). The analysis is shown schematically in **8**;

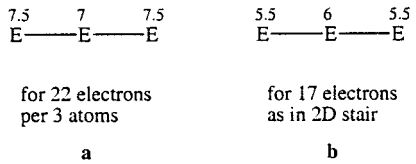


**8**

in the triatomic, the electron distribution is roughly as in **8a**; three-center electron-rich bonding, in a Hückel model, leads to accumulation of a 0.5 $e^-$ at the end atoms.[9] This follows from the orbitals in **3**; the lowest MO distributes its electrons approximately 0.5, 1.0, 0.5 along the triatomic, the HOMO 1.0, 0.0, 1.0.

Subsequent oxidation by 1 electron at the ends of the triatomics during the *Aufbau*, and at every atom by 1 electron,

(9) Lipscomb, W. N. *Boron Hydrides*; W.A. Benjamin, Inc.: New York Amsterdam, 1963; pp 30−32.

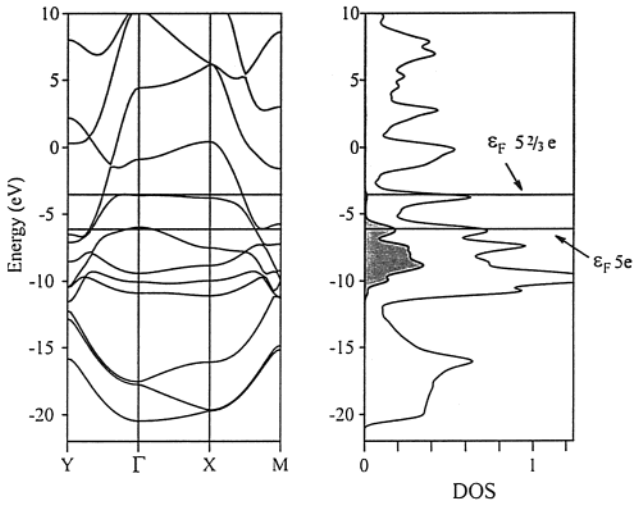


**Figure 2.** Band structure of the stair **2** (left) and contribution of the $p_z$ orbital of the $Sn_{sq}$ atom to the total DOS (right). The figure also shows the Fermi level for the experimental electron count of 5 electrons/atom and for the extended Zintl−Klemm electron count of $5^2/_3$ electrons/atom.

makes the "central" square atom more negative (for a $5^2/_3$ average electron count). This is shown in **8b**, where the numbers are the approximate number of electrons not in the triatomic molecule, but in the triatomic unit of the 2D stair. We can also say that the electron excess at the central atom is likely to be in the $p_z$ orbital. Indeed, none of the oxidation steps (which we detailed above) in the construction of more complex structures from a 0D triatomic involves this orbital.

The two constructions we chose are not unique. One may assemble these slabs in still other ways—in a separate paper dealing with $X_5$ structures we show still another way.[10]

We have thus reached an interesting point—the extended Zintl−Klemm picture clearly leads us (in several ways) to expect $5^2/_3$ electrons per Sn. But the experimentally observed $Sn^-$ slabs have an electron count of 5. Let us look at the electronic structure of the stepped $Sn^-$ slabs and see if we can reconcile these two viewpoints.

**Band Structure of the 2D Sn slab of LiSn.** We model the sheet with all Sn−Sn distances equal to 3.17 Å (an average of the Sn−Sn distances in the tread of observed structure) and all step angles at 105°. The assumption of equal bond lengths allows us to compare the strength of the distinct bonds in the structure—if the overlap population of a given bond is then large or small (despite the fact the underlying bond length is the same), that is a hint of a bonding proclivity inherent in the structure. The band structure of the 2D slab is reported in Figure 2. The Fermi level ($\epsilon_F$) for both 5 and $5^2/_3$ electron counts is shown. We note first that the 2D net appears in the calculations to be metallic, $\epsilon_F$ lying in a region of moderate DOS. The net would also be metallic for the hypothetical $5^2/_3$ electron count.

What is the nature of the states near the Fermi level and the charge distribution in the sheet? The square planar atom in fact is more negative; the Mulliken charges are $Sn_{bu}$ (−0.86), $Sn_{sq}$ (−1.28). For the observed electron count of 5 the population of $p_z$ of $Sn_{sq}$ is computed as 1.82.

Let us examine the bonding in the sheet, as gauged by the integrated crystal orbital overlap population (COOP) for the Sn−Sn bond, reported in **9**. For reference, the Sn−Sn overlap population (OP) at a distance of 3.17 Å for a singly bonded $H_3Sn-SnH_3$ molecular model with the same Sn−Sn distance is 0.62.

(10) Ienco, A.; Hoffmann, R., unpublished results.

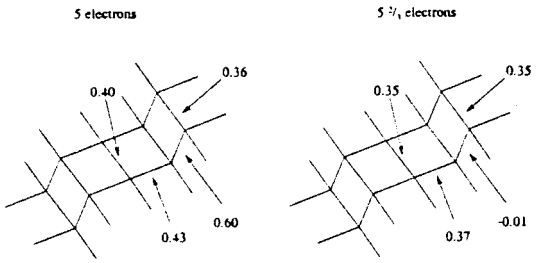


**9**

In the case of 5 electrons per Sn, the highest value of the COOP (0.60, by far the largest in the structure) corresponds to the experimentally shortest (2.99 Å) Sn−Sn distance, the one for the interstep $Sn_{bu}-Sn_{bu}$" bond. Recall that in our model all Sn−Sn bond lengths are equal, so differences as marked as the ones observed are indicators of real differentials in bonding. That magnitude of the COOP is also quite consistent with the value of the OP for the single Sn−Sn bond model. The three other symmetry-distinct interactions have lower OPs, consistent with the existence of hypervalent bonding between the Sn atoms.

We now come to a crucial point; If the electron count were $5^2/_3$, the bonding would be *very* different. Such an electron count (see **9** right) leads to an almost zero OP (−0.01) between the butterfly atoms, indicative of essentially no interaction. If the electron count were $5^2/_3$, the slab would better described as a series of noninteracting treads (as in **10**). A breakdown of the

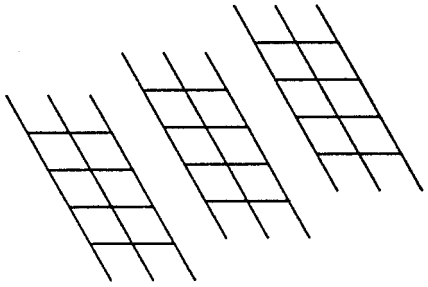

**10**

COOP (not shown here) shows that the calculated repulsion derives mainly from the $p_z$ orbital combination of the $Sn_{bu}$ atoms.

While the near-zero $Sn_{bu}-Sn_{bu}$" COOP helps us to understand why the system at hand does not take up (through variation of stoichiometry) the $5^2/_3$ electron count, it is important, we feel, to understand the origin of the effect better. To explore this, it is instructive to take a look at other hypervalent slabs.

**Hypervalent Slabs of Different Geometry, and for Different Elements.** Let us consider the square planar and the zigzag slab shown in **11**. As pointed out in other work,[7] the

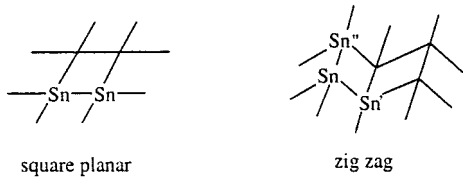


**11**

preferred electron count for the square planar net is 6 electrons per atom and for the "zigzag" net is 5. To allow a comparison with the net studied early in this paper, the Sn−Sn distances in the calculation are fixed to 3.17 Å and the zigzag angle to 105°.

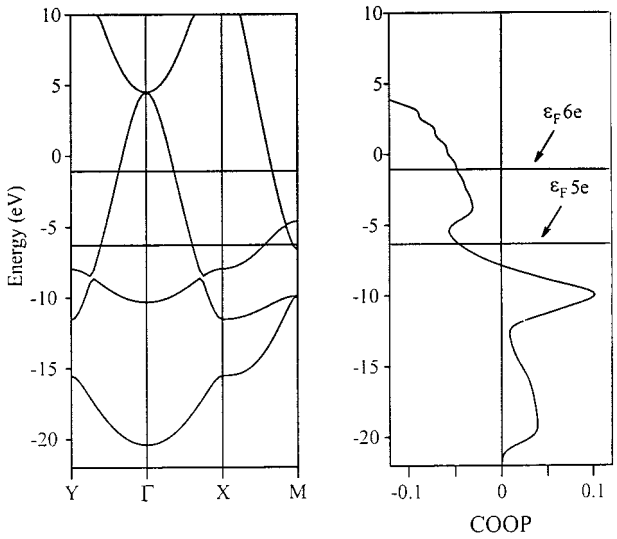


**Figure 3.** Band structure of the square planar net **11** (left), and COOP curve for the Sn−Sn interaction (right). The Fermi level for electron counts of 5 and 6 is shown.

The band structure of the square planar slab is reported in Figure 3. Fermi levels for 5 and 6 electrons are shown. The net is metallic. The value of the OP for the Sn−Sn bond is 0.45 for an electron count of 5 electrons, while it is 0.20 for 6 electrons. The latter value indicates a rather weak interaction, compared with the value for the hypervalent linkage in the stair (see **9**). The COOP diagram for the Sn−Sn bonds (Figure 3) reveals that the Sn−Sn repulsion for the electron count of 6 derives from orbital combinations with energy higher than −7.5 eV. In this region of energy, one is occupying levels which are strongly antibonding.

The zigzag slab is also metallic. For an electron count of 5 electrons, the OP for the single bond Sn−Sn′ is 0.53, while for the hypervalent bond Sn−Sn" it is 0.28. The comparison of the values of the OP of the zigzag slab with the ones of the 2D stair (see **9**) shows that the electron-rich linkages (Sn−Sn") in the zigzag slab are weaker than in the stair slab ($Sn_{sq}-Sn_{sq}'$ and $Sn_{bu}-Sn_{bu}'$).

In Figure 4, the COOP curves for the Sn−Sn′ single bond and the Sn−Sn" hypervalent bond are reported. Just as in the case of the stair, the addition of electrons to the sheet increases the strength of the hypervalent linkage, but reduces markedly the population of the single bond. In analogy with the stair, chemical reduction of the net leads to separate linear chains of Sn atoms.

We also want to compare the total energy of the three networks (square planar, zigzag, stair) for the electron count of 5 per Sn atom. The square planar net is calculated 0.07 eV per Sn atom more stable than the stair and 0.36 eV more stable than the zigzag. This is in disagreement with the observed structure; either the computational method is inadequate or the countercation role is significant in determining the structure.

So far we have a discouraging set of negative results. We begin to obtain some insight into the problem from a comparison of the total energy difference of the slabs for other main group elements of the same row as Sn (In, Sb, Te). In this context, it is also instructive to explore not only the electron count of 5 but also a larger range of electron counts. In the calculations we used a distance of 3.25 Å for In (as in the structure of elemental In), while for Sb and Te we reduce the distances to 3.14 and 3.11 Å, respectively, to take into account the smaller size of these two atoms relative to the Sn atom.

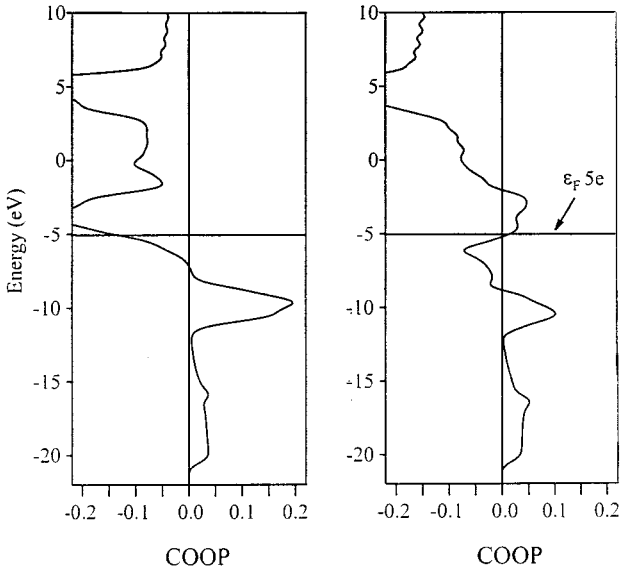


**Figure 4.** COOP curves of the Sn−Sn′ single bond (left) and of the Sn−Sn" hypervalent bond (right) in the zigzag slab **11**. The Fermi level for an electron count of 5 electrons per atom is shown.

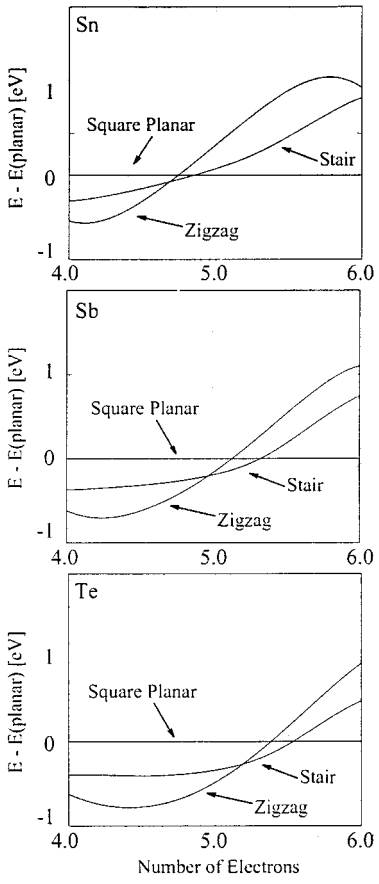


**Figure 5.** How the energy of the three nets of fifth row elements (Sn to Te) varies as a function of electron count.

Figure 5 reports the total energy of the Sn, Sb, and Te slabs (the In results are not shown in the figure; they are much like Sn) for an electron count of 4−6. The square planar slab geometry is the arbitrary zero reference, shown by a straight line. The curves each contain a region of high electron counts where the zigzag and stair slabs are less stable than the square planar one and a region of low electron counts where these are preferred. The crossing point of the stair total energy curve with the square planar curve changes from 4.5 in the indium and tin cases to a little bit more than 5.5 in the tellurium one. The stair itself is most stable only in a small range of electron counts. This range increases from In to the Te. It appears that as we move toward the right side of the periodic table, the extended Zintl−Klemm-type picture works better. From Figure 5, it is also clear that a 5-electron slab of Sb has more chances to take on a stair conformation, while a slab of Te prefers the zigzag geometry.

When we look at the Te stair net in more detail (for an electron count of $5^2/_3$), we find an important clue. The COOP for the Te−Te bonds (shown in **12**) reveals that all the

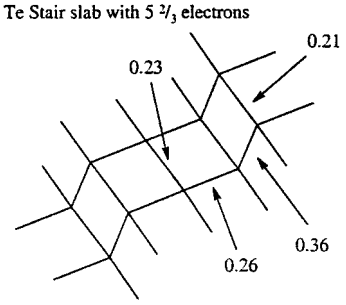


**12**

interactions are positive! Notice that the COOP of the $Te_{bu}$−$Te_{bu}$″ bond is *positive* (0.36), whereas the $Sn_{bu}$−$Sn_{bu}$″ COOP for that same electron count was near zero (see **9**). Obviously there is a big difference between $Sn^{2-}$ and Te, even if the electron count in the structures formed by both elements is the same. This difference we need to understand.

We might note here what is known about Sn square planar slabs in other phases. A detailed analysis for the fourth group element square sheets was presented by two of us as part of a comprehensive study of multicenter electron-rich bonding in extended systems.[7] There are a good number of such phases: i.e., $M^{IV}X_2$ (M = Zr, Ti, Hf, U, Th; X = Si, Ge, Sn), $RESn_2$, $RECu_2Sn_2$ (RE = rare earth), etc. For Sn, the electron count can vary between 5 and 6 electrons per atoms. When the electron count is lower than 6, the square sheets appear to turn on interactions with other surrounding electron-rich structural motifs and/or isolated atoms. For details, the reader is referred to the Papoian and Hoffmann paper.[7]

Figure 5 is instructive in another way, in that it suggests what sheet deformations are likely for different electron counts. Consider $Li_nSn$, with a potentially variable Li content. If the Sn sublattice forms sheets (it does not have to), a square sheet should be preferred for $n > 1$, a square sheet or stair for $n = 1$, and a zigzag structure for $n < 1$.

**Differences in Electron-Rich Multicenter Bonding as One Moves across the Periodic Table.** Two anomalies confront us: (1) The usually reliable extended Zintl−Klemm concepts lead to an electron count for the 2D slab ($5^2/_3$) which is higher than that observed; (2) For that electron count ($5^2/_3$), one stair overlap population (usually a reliable indicator of bonding) is actually slightly negative, near zero.

The previous section provides us with an important clue in the comparison of isoelectronic element structures, in particular $Sn^{2-}$ and Te—small overlap populations between bonded atoms are observed only for $Sn^{2-}$ and not for Te. We proceed to trace the origins for the difference back to increasingly simpler systems.

Our first step is to examine the 1D tread of Figure 1. The extended Zintl−Klemm count there is $6^1/_3$ per atom. **13**

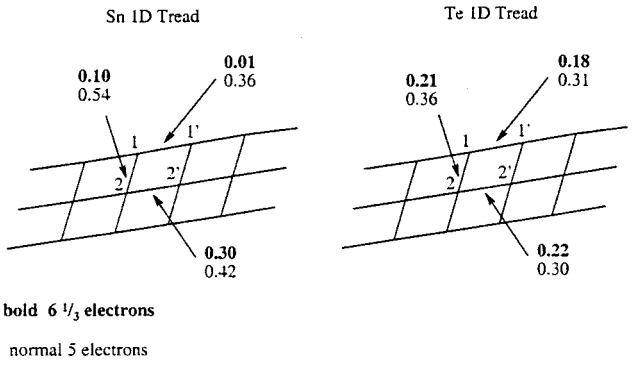


**13**

compares the calculated OP's for that count and for the lower one of 5 electrons per atom.

Note the great discrepancy between Sn (some very small COOPs) and Te for the $6^1/_3$ electron count. For 5 electrons per main group element instead, all the Sn−Sn COOP values are approximately of the same magnitude and comparable with the value for the hypervalent Sn−Sn bond in the stair. On the other hand, for the Te net, the values of the COOP at even the $6^1/_3$ electrons are substantial, comparable with those in a hypervalent molecular model $Te_3^{4-}$also calculated and with the values reported for the 2D slab of Te (see **12**).

Similar results are obtained for the 1D stair, where the extended Zintl−Klemm count is $6^2/_3$ per atom. **14** shows the

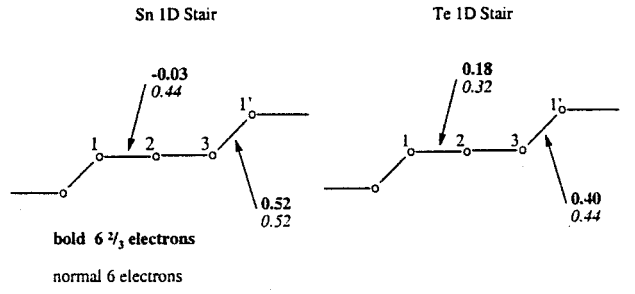


**14**

Sn and Te 1D stairs, with the calculated OPs for $6^2/_3$ and 6 electrons. One Sn OP is slightly negative for the higher electron count. Once again, the extended Zintl−Klemm count leads to no interactions in the stair if it is built up from Sn atoms.

We retreat to the fundamental building block of all these systems, the linear triatomic. As shown in **15**, a calculation on

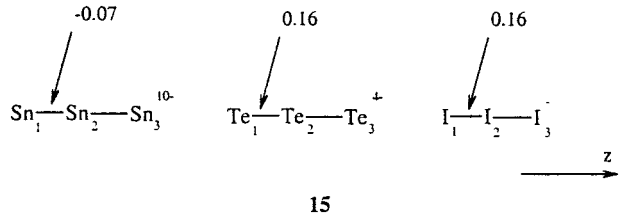


**15**

the 22-electron $Sn_3^{10-}$ molecule gives an OP of −0.07 for the Sn−Sn bond, while for Te−Te and I−I the OP is 0.16 and 0.16 (in $Te_3^{4-}$, and $I_3^-$, respectively). We fixed the bond distances at 3.17 Å for the $Sn_3^{10-}$, 3.11 Å for $Te_3^{4-}$, and 3.00 Å for $I_3^-$.

Where does the Sn−Sn antibonding come from? The interaction diagram of Figure 6 shows the energy levels and some of the orbitals of $Sn_3^{10-}$ system. The main features of this diagram are also common to $Te_3^{4-}$ and $I_3^-$. We construct the orbitals of the composite system by interacting a $\sigma_s$ set (the three s orbitals,

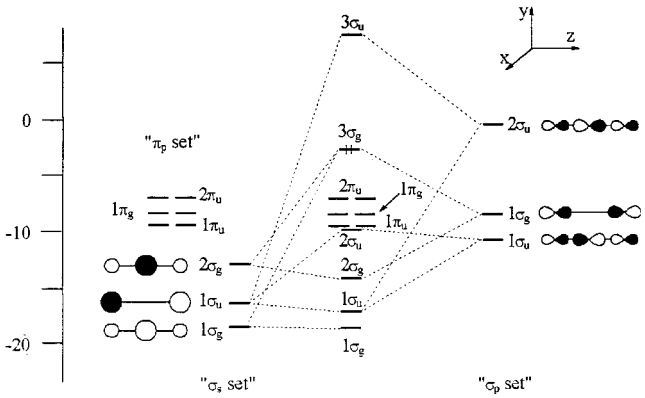


**Figure 6.** Interaction diagram for triatomic $Sn_3^{10-}$. The orbitals of the triatomic molecule are built from three sets of orbitals. The $\sigma_s$ set includes only the s atomic orbitals, the $\sigma_p$ set the $p_z$ atomic orbitals, and the $\pi_p$ set the $p_x$, $p_y$ atomic orbitals. Symmetry allows interactions only between the $\sigma_s$ set and the $\sigma_p$ set.

all filled), a $\pi$ set ($p_x$, $p_y$, all filled), and the $\sigma_p$ set ($p_z$ the three-center system, all but one MO occupied). First (left and right in Figure 6) within each set ($\sigma_s$, $\pi$, $\sigma_p$) is tuned on, and then the $\sigma_s$, $\sigma_p$ mixing is allowed.

One source of repulsion might be the filled $\pi$ set of 12 electrons. The contributions of these orbitals to the OP are −0.07 (Sn) to −0.01 (I). So part of the differential is here.

But the greater part of the special destabilization of the Sn system is due to s,p mixing. Take a look at the HOMO of $Sn_3^{10-}$. **16** shows one contour of this HOMO. It is derived from the

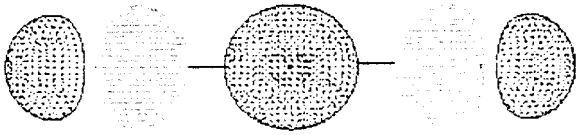

**16**

formally nonbonding three-center $\sigma_p$ set. But note how destabilized it is in Figure 6. The destabilization is due to the antibonding mixing in of central atom s orbital, i.e., to s,p overlap.

In fact, the contribution of the two electrons in this *one* MO to the total OP is −0.48 (Sn), −0.17 (Te), and −0.12 (I). And if one does a calculation for the triatomics with all s,p interactions set to zero, the contribution of this orbital at the OP is zero for all triatomics, and one obtains a much more even set of OPs: 0.18 (Sn), 0.22 (Te), and 0.20 (I). Our conclusion is that s,p mixing, operating mainly through this HOMO, is the main factor responsible for destabilizing the Sn system relative to the isoelectronic I (or Te) one.

More generally, it is clear that hypervalent bonding, for the same electron count, should be much weaker for Sn than for I, and in general, such bonding should be increasingly problematic as one moves from the right toward the middle of the periodic table in any period. What is a reasonable electron count (and that is what the extended Zintl−Klemm counting gives) for I, $Te^-$, and $Sb^{2-}$ will not be a good one, but would result in too much antibonding, for isoelectronic $Sn^{3-}$. This is the primary reason for the low actual electron counts in the Sn sheets.

While s,p mixing has been studied by us[7,11] and by others[12] as one goes up and down a group, the effect at hand is moving

(11) Seo, D.-K.; Hoffmann, R. *J. Solid State Chem.* **1999**, *147*, 26.

(12) see for instance: Albright, T.; Burdett, J.; Whangbo, M.-H. *Orbital Interactions in Chemistry*; John Wiley & Sons: New York, 1985; Chapter 6.

**Table 1.** Extended Hückel Parameters (eV for $H_{ii}$) Used in the Calculations

| | $H_{ss}$ | $H_{pp}$ | $\zeta_s$ | $\zeta_p$ |
|---|---|---|---|---|
| In | −12.60 | −6.19 | 1.903 | 1.677 |
| Sn | −16.16 | −8.32 | 2.12 | 1.82 |
| Sb | −18.80 | −11.70 | 2.323 | 1.999 |
| Te | −20.80 | −14.80 | 2.51 | 2.16 |
| I | −18.00 | −12.70 | 2.679 | 2.322 |
| Li | −5.4 | −3.5 | 0.65 | 0.65 |

**Table 2.** OP for the Triatomic Molecule as a Function of the Variation of the Extended Hükel Parameters from Sn to Te Atom[a]

| | Sn | | | | Te | | | | |
|---|---|---|---|---|---|---|---|---|---|
| | $H_{ss}$ | $H_{pp}$ | $\zeta_s$ | $\zeta_p$ | $H_{ss}$ | $H_{pp}$ | $\zeta_s$ | $\zeta_p$ | OP |
| 1 | x | x | x | x | | | | | −0.074 |
| 2 | | x | x | x | x | | | | −0.087 |
| 3 | | | x | x | x | x | | | −0.058 |
| 4 | x | x | | x | | | x | | 0.087 |
| 5 | | x | | x | x | | x | | 0.095 |
| 6 | | | | x | x | x | x | | 0.105 |
| 7 | x | x | | | | | x | x | 0.157 |
| 8 | | x | | | x | | x | x | 0.152 |
| 9 | | | | | x | x | x | x | 0.167 |

[a] An "x" indicates the parameters used in each calculation. The end points are respectively the $Sn_3^{10-}$ and the $Te_3^{4-}$ molecules.

across a period. Is it the absolute energy, the separation, or the extent in space of the ns and np orbitals, that matters? To elucidate this point, we recalculate the triatomic system, varying the orbital parameters of Sn and Te and observing the effect on the OP.

In the extended Hückel method, the ionization potential $H_{ii}$ is a measure of the energy of an orbital and the Slater coefficient $\zeta_i$ is related to the orbital extension. The parameters used in the calculations are reported in Table 1. From In to I, the values of $H_{ii}$'s decrease, but the difference between the $H_{ss}$ and $H_{pp}$ remains almost constant in the series. The orbitals definitely became more contracted as one moves across a period.

In Table 2 we show a series of numerical experiments in which we interchange in a symmetrical way the $H_{ii}$ and the $\zeta$ parameters of Sn and Te atom. (We fixed the distance at 3.17 Å in all the calculations). In this way, we can evaluate the relative magnitude of the various contributions, following the OP of the system. The calculations are divided in three series of three calculations in which we fix the $\zeta_s$ and $\zeta_p$ parameters and use different set of $H_{ii}$. The "end points" are the Sn system (negative Sn−Sn OP of −0.074) and Te (positive OP, 0.167). The *x* indicates the value of the parameters used; the geometries and the electron counts are identical. For each case, we give the OP that emerges from calculation.

It turns out that variation of the $H_{ii}$ is much less important than the contraction of the orbitals. We also notice that a larger difference between $H_{ss}$ and $H_{pp}$ destabilizes the bond, and for the same difference, a larger total sum of the $H_{ss}$ and $H_{pp}$ increases the strength of the bond.

If the orbital exponents in Table 1 are to be taken at face value, one may naturally suggest that s orbitals contract faster than p orbitals on the right side of the periodic table, thus, leading to the smaller s,p overlap and mixing. However, relativistic Dirac−Fock calculations of the maximums of atomic orbital radial densities in the In−I series show the opposite trend; i.e., the s and p orbitals are better matched in size for I than for In (see Table 3).[13]

**Table 3.** Radius of Maximum Radial Density for s and p Valence Orbitals As Calculated from Dirac−Fock Wavefunctions ($p_{1/2}$ and $p_{3/2}$ Values Are Averaged)[a]

| | In | Sn | Sb | Te | I | ref |
|---|---|---|---|---|---|---|
| $R_s$ | 1.18 | 1.10 | 1.03 | 0.96 | 0.92 | 13 |
| $R_p$ | 1.56 | 1.37 | 1.24 | 1.15 | 1.07 | 13 |
| $R_p - R_s$ | 0.38 | 0.27 | 0.21 | 0.19 | 0.15 | 13 |
| $R_{at}$ (theor) | 1.37 | 1.24 | 1.14 | 1.06 | 1.00 | 14 |
| $R_{at}$ (emp) | 1.55 | 1.45 | 1.45 | 1.40 | 1.40 | 14 |

[a] $R_{at}$ are theoretical and empirical atomic radii. All values are given in angströms.

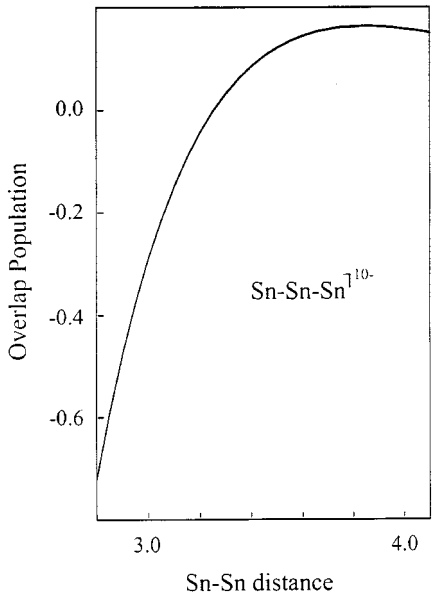


**Figure 7.** Sn−Sn overlap population (OP) for $Sn_3^{10-}$ as function of the Sn−Sn distance.

We have come to a startling conclusion—the $H_{ii}$ parameters do not play a significant role in determining the extent of s,p mixing, while the relative sizes of s and p orbitals seem to suggest that s,p mixing is greater on the right side. We believe that the following reasoning, somewhat speculative in nature, may help to resolve this inconsistency.

It is apparent from Table 3 that both s and p orbitals contract significantly from In to I. If one assumed that the average of s and p orbital density maximums are indicative of the atomic size, then one would expect a 0.37-Å diminution of atomic radii when going from In to I (see Table 3). However, the empirical atomic radii compiled by Slater suggest much smaller contraction (Table 3).[14] While at present we do not have an explanation for this effect, it nevertheless helps to rationalize the suggestion of smaller s,p mixing for Te and I compared to In and Sn.

Indeed, not only the relative size of s and p orbitals determines the extent of s,p mixing but also the effective distance between two atoms (i.e. smaller distance leads to larger overlap and mixing). To examine the role of this factor, we recalculated the Sn−Sn overlap population values in $Sn_3^{10-}$ as function of Sn−Sn distance. As is clearly seen from Figure 7, the OP increases monotonically with increasing distance, a result that might appear counterintuitive (the OP will go down eventually). We trace this result to the influence of the "antibonding" hypervalent MO depicted in **16**—the greater Sn−Sn separation decreases the s,p overlap, and thus the magnitude of s,p-mixing, which in turn diminishes the antibonding character of this molecular orbital. Therefore, on moving from left to right in the periodic

(13) Desclaux, J. P. *At. Data Nucl. Data Tables* **1973**, *12*, 311.

(14) Slater, J. C. *J. Chem. Phys.* **1964**, *41*, 3199.

table, the *effective* distance (relative to the size of the atoms) between bonded atoms increases, leading to less s,p overlap and s,p mixing. The reader is also referred here to an important paper on s,p bonding in main group elements.[15]

Our conclusion is that the observed lowering of the electron count in the hypervalent Sn slabs—in response to antibonding orbital repulsion for that would be a "normal" hypervalent electron count—is connected to the diffuseness of the Sn orbitals.

**The 3D Structure and the Role of the Countercation.** Let us now return to a previous troublesome point, the stability of the square planar slab (**11**) with respect to the 2D stair one (**1**). We found that for an electron count of 5 and 6 electrons the square sheet was favored. We now build up from the 2D sheet to the full structure. First, we examine the full 3D structure, but without the Li atoms. The band structure (not reported here) is very similar to that shown in Figure 2. Also, the Mulliken charge of the Sn atoms and the COOPs for the Sn−Sn bonds have the same value as in the 2D stair model. There is a very small bonding interaction between the $Sn_{sq}$ and $Sn_{bu}$ of two adjacent layers. (COOP = 0.03). Clearly the system is quite two-dimensional in its Sn sublattice.

So we have to include the Li atoms in the calculations. The importance of the Li atom for the final structure lies in its small ionic radius. This is clear from looking at the whole series of the binary alkali-tin (1:1) phases. The crystal structures of NaSn, KSn, RbSn, and CsSn contain a (more or less) distorted tetrahedral cluster of $Sn_4^{4-}$ (isoelectronic with $P_4$).[16] As remarked previously, only for LiSn is this structural motif unknown. Also, the authors of a recent paper[17] on liquid alkali-tin alloys demonstrated that in LiSn solution the $Sn_4^{4-}$ tetrahedron is unstable. Due to the small size of the Li ion, Sn intercluster interactions are made possiblr and destabilize the intracluster bond.

We were reluctant to include the Li atoms in the calculation, because of the well-known problems in the choice of parameters for the alkali metal. For Li, the set of extended Hückel parameters derived from metal atoms has the 2s and 2p orbitals too low in energy and quite diffuse. The result is too much interaction with the Sn atoms. We prefer to use a parameter set that has orbitals with higher energy and a little less diffuse. This is in order to have some interaction but not an excessive amount. In general, questions about Li and $Li^+$ parameters in extended Hückel calculations render problematic calculations on this element.

The band structure, total DOS, and Li contribution of the 3D stair with lithium atoms are reported in Figure 8. Below the Fermi level, the larger contribution of the Li atoms to the total DOS is around −10 eV. The integrated lithium contribution to the total DOS is around 4%.

The COOP values in the 3D stair are shown schematically in **17**. All the Li−Li interactions, not reported in **17**, are almost zero. The $Sn_{sq}$−$Sb_{sq}$ and the $Sn_{bu}$−$Sn_{bu}$ bonds have the same strength. There are small bonding Li−Sn interactions. The $Sn_{sq}$ interactions with neighbor Li atoms have the same strength, while for the $Sn_{bu}$, one Sn−Li interaction is larger than the other two. $Sn_{sq}$ has its lone pair ($p_z$) symmetrically interacting with all the Li atoms, while $Sn_{bu}$ atom instead has its lone pair localized in the direction of only one of the Li atoms.

Let us take a look at the electron distribution in the slab. The $Li_{bu}$ and $Li_{sq}$ atoms carry a charge of +0.56 and +0.59, respectively, while $Sn_{bu}$ and $Sn_{sq}$ are negatively charged, −0.53 and −0.65, respectively. If we use the Mulliken charges as a reasonably realistic measure of the actual electron count on the Sn slab (and we are cautious about this), we obtain an electron count of 4.6 electrons per Sn atom. Please look at Figure 5 again. For Sn with an electron count lower than 5, the 2D stair is more stable than the square planar. This result, we think, is also an indication of the importance of the Li atoms not only crystallochemically (i.e., the consequences of their small size) but also in setting the degree of electron transfer which makes one or another crystal geometry possible.

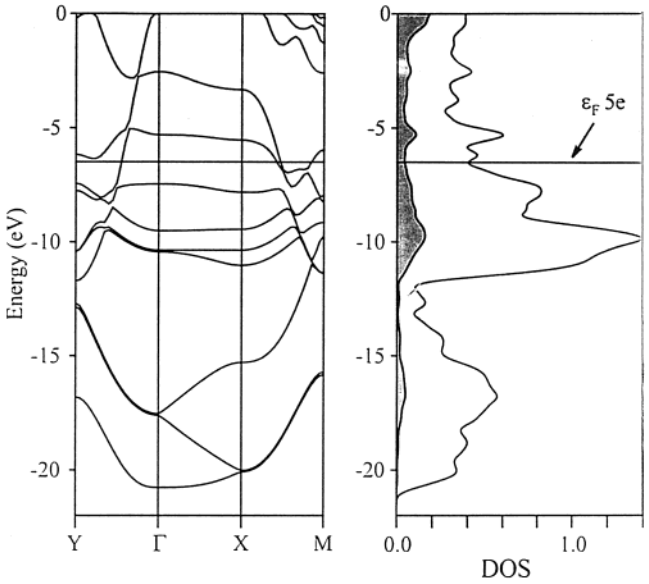


**Figure 8.** Band structure of the 3D crystal (left) and the contribution of the Li atoms at the total DOS (right). The Fermi level for an electron count of 5 electrons/atom is also shown.

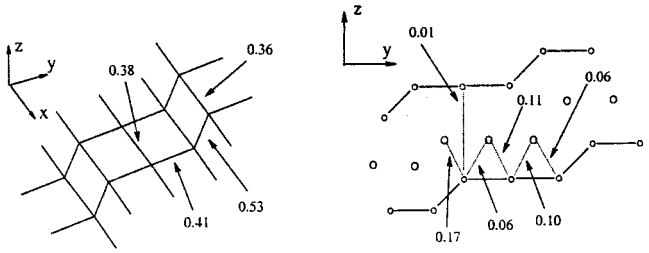


**17**

## Concluding Remarks

What began as a series of theoretical defeats turned into a puzzle. One that in turn led to what we believe is a net gain in our understanding. The unusual 2D Sn sublattice in Li did not have an electron count that fits the usually reliable extended Zintl−Klemm number ($5^2/_3$ electrons per Sn) appropriate for the geometry observed and derived in two different ways. In fact, in our calculations the extended or electron-rich Zintl−Klemm electron count led to some completely broken bonds.

A methodical tracing back of this effect led to a surprise—isoelectronic electron-rich Sn, Sb, Te, and I compounds differed tremendously in their bonding strength. What was reasonable bonding for Sb, Te, and I was not such for Sn. We found that the primary source of the differential lay in antibonding interactions in the HOMO of the electron-rich three-center bond. For the same electron count, the antibonding in the HOMO is greater for Sn than I. This in turn could be traced to greater s,p mixing for Sn, and that was due to the relative diffuseness of the Sn valence orbitals.

(15) Kutzelnigg, W. *Angew. Chem., Int. Ed.* **1984**, *23*, 272.
(16) Müller, W.; Volk, K.*Z. Naturforsch.* **1977**, *32B*, 709. Hewaidy, I. F.; Busmann, E.; Klemm, W. *Z. Anorg. Allg. Chem.* **1964**, *328*, 283.
(17) Genser O., Hafner J. *J. Non-Cryst. Solids* **1999**, *250*−*252*, 236.

The effect has to be quite general. *s,p mixing will diminish as one moves across a period. And extended, electron-rich Zintl−Klemm electron counts that are "correct" for the right side of a main group sequence (groups 15−17) are likely to weaken bonding interactions in electron-rich systems for group 14 elements.* For such molecules or extended system, we believe that in general the preferred electron count will be lowered from the extended electron-rich Zintl−Klemm one.

In a further suggestive finding, the Li ions in the lattice are not only likely to influence the structure by their small size but may also tune the actual electron count on the anionic sheet.

## Computational Details

The calculations presented in this work are in the framework of the extended Hückel[18] tight-binding method.[19] Either the YAeHMOP[20] and CACAO[21] software packages were used. The parameters used in the calculations are listed in Table 2. The off-diagonal elements of the Hamiltonian were evaluated with the Wolfsberg−Helmoholtz formula.[22] Numerical integrations over the symmetry-unique section of the Brillouin zone of the two-dimension structure were performed using a set of 400k-points. The three-dimensional calculations used 500k-points.

**Acknowledgment.** We are grateful to the National Science Foundation for its support of this work by the Research Grant CHE 99-70084.

JA0032576

(18) Hoffmann, R.; Lipscomb, W. N. *J. Chem. Phys.* **1962**, *36*, 2179. Hoffmann, R.; Lipscomb, W. N. *J. Chem. Phys.* **1962**, *36*, 3489. Hoffmann, R.; Lipscomb, W. N. *J. Chem. Phys.* **1963**, *37*, 590. Hoffmann, R. *J. Chem. Phys.* **1963**, *39*, 1397.

(19) Whangbo, M.-H.; Hoffmann, R.; Woodward, R. B. *Proc. R. Soc. London, Ser. A* **1979**, *366*, 23. Whangbo, M.-H.; Hoffmann, R. *J. Am. Chem. Soc.* **1978**, *100*, 6093.

(20) Landrum, G. A.; Glassey, W. V. YAeHMOP (version 3.0). The YAeHMOP is freely avalaible on the WWW at http://overlap.chem.cornell.edu:8080/yaehmop.html.

(21) (a) Mealli, C.; Proserpio, D. M. *J. Chem. Educ.* **1990**, *67*, 399. (b) Mealli, C.; Ienco, A.; Proserpio, D. M. *Book of Abstracts of the XXXIII ICCC*, Florence, Italy, 1998; Abstr. 510.

(22) Ammeter, J. H.; Elian, M.; Summerville, R. H.; Hoffmann, R. *J. Am. Chem. Soc.* **1978**, *100*, 3686.